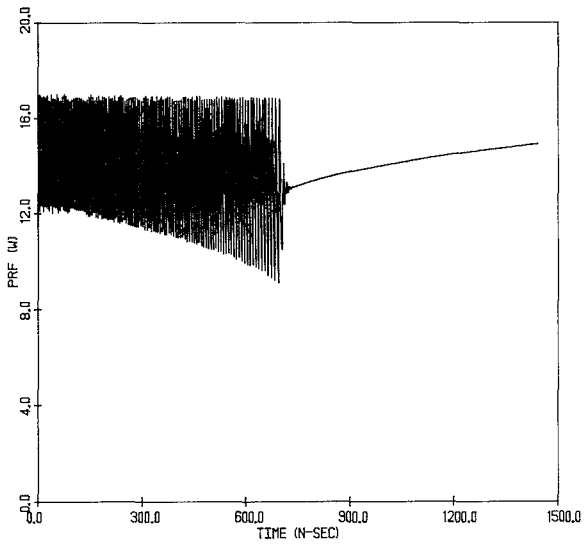

Fig. 10. RF power for the injection-locked case ($J_{dc} = 646$ A/cm^2, $\tau = 8$ μs, $I_L = 0.341$ A, $P_{in} = 1.5$ W and $f_0 = 10$ GHz).

RF power generated by the diode is

$$P_{RF} = -\tfrac{1}{2} G_D V_{RF}^2 \tag{7}$$

where $G_D = \mathrm{Re}\{Y_D(V_{RF})\}$. The expressions in (6) and (7) are plotted in Fig. 9. It is seen that as I_L is varied from 300 A/cm^2 (0.39 A) to 800 A/cm^2 (1.04 A), the RF power first increases, reaches a maximum for $I_L = 450$ A/cm^2 (0.585 A), and then decreases. (P_{RF} in Fig. 9 is the RF power at the start of the pulse, whereas the RF power in Table II is the average over the 1.5-μs pulse width.) Below $I_L \cong 285$ A/cm^2 (0.370 A, $P_{in} = 1.76$ W), it is anticipated from Fig. 9 that locking cannot occur except perhaps at very low P_{RF} values. (It must also be investigated whether the operating points in Fig. 9 are stable.) This expectation is borne out by the simulation in Fig. 10 for which $P_{in} = 1.5$ W ($I_L = 0.341$ A). The diode does not lock until it has heated up to 477°K, so that the curves in Fig. 9 are no longer applicable. As the diode continues to heat up, the generated RF power gradually increases to 14.9 W. This behavior is consistent with the experimental results, since for P_{in} much below 2 W the locking at 10 GHz was not found to be stable.

VI. Conclusions

It has been shown that a large-signal IMPATT diode simulation program employing the drift-diffusion approximation in conjunction with a quasi-static transient simulation can accurately predict experimentally observed behavior at 10 GHz, both for the free-running and injection-locked cases. These programs may be used for diode and circuit design at higher frequencies where measurements become more difficult. However, it may be necessary to include relaxation effects in the IMPATT diode simulation since it has been shown that these effects become significant at low millimeter-wave frequencies [7].

References

[1] K. Kurokawa, "Injection locking of microwave solid-state oscillators," *Proc. IEEE*, vol. 61, pp 1386–1410, Oct 1973.

[2] R. K. Mains, G I. Haddad, and D. F. Peterson, "Simulation of pulsed IMPATT oscillators and injection-locked amplifiers," Tech. Report No. AFWAL-TR-81-1177, Electron Physics Laboratory, University of Michigan, Ann Arbor, Feb. 1981.

[3] P. E. Bauhahn and G. I. Haddad, "IMPATT device simulation and properties," *IEEE Trans. Electron Devices*, vol. ED-24, pp. 634–642, June 1977.

[4] P. E. Bauhahn, "Properties of semiconductor materials and microwave transit-time devices," Ph.D. dissertation, University of Michigan, Ann Arbor, Oct. 1977.

[5] R. K. Mains and G. I. Haddad, "Properties of high-efficiency X-band GaAs IMPATT diodes," Tech. Report No. AFWAL-TR-81-1066, Electron Physics Laboratory, University of Michigan, Ann Arbor, June 1981.

[6] L. H Holway, Jr., "Transient temperature behavior in pulsed double-drift IMPATT diodes," *IEEE Trans. Electron Devices*, vol. ED-27, pp. 433–442, Feb. 1980.

[7] R. K Mains and G. I. Haddad, "Simulation of GaAs IMPATT diodes including energy and velocity transport equations," in *1983 WOCSEMMAD Conf.*, (San Antonio, TX), Feb 1983.

Spectral Domain Analysis of an Elliptic Microstrip Ring Resonator

ARVIND K. SHARMA, MEMBER, IEEE

***Abstract*—The quasi-static capacitance of an elliptic microstrip ring resonator is evaluated with the spectral domain technique. The effect of fringing of fields associated with the structure is determined using this capacitance value in terms of the effective eccentricities of the inner and outer ellipses, the effective values of the ratio of the semimajor and semiminor axes, and the effective dielectric constant. The resonant frequency of the even TM_{c110} mode, calculated utilizing them, is in good agreement with the experiment. Mode charts for the dominant and higher order even and odd TM_{cm10} resonance modes are also presented.**

I. Introduction

Of the various microstrip resonant structures, those with simple geometrical shapes have emerged as the most popular resonant structures in practice. Rectangular, circular disk, and ring resonators, therefore, find extensive applications in oscillators, filters, and circulators. On the other hand, microstrip resonant structures of complex geometrical shapes have not received much attention to date. This mainly is due to inadequate design information available in the literature.

The resonant structures of complex geometrical shapes, in general, provide better performance and greater flexibility in the design. This has been demonstrated for the equilateral triangular microstrip element and the regular hexagonal element in filter and circulator applications [1]–[3]. Although some preliminary results are available, they must be analyzed in greater detail so that they can be meaningfully incorporated into the design of MIC components. With this objective in mind, several different geometrical shapes have recently been investigated in detail [2]–[6].

The elliptic microstrip disk and ring resonators have the potential for being used in practical microwave integrated circuits. The elliptic microstrip disk [6]–[8] can be utilized in harmonic multipliers and parametric amplifiers, since there exists a harmonic relationship between mode frequencies. It also can be used as an antenna element to achieve circular polarization [9]. The elliptic

Manuscript received July 13, 1983; revised September 19, 1983

The author is with the Microwave Technology Center, RCA Laboratories, David Sarnoff Research Center, Princeton, NJ 08540.

0018-9480/84/0200-0212$01.00 ©1984 IEEE

microstrip ring resonator [10], [11] is a general structure which reduces to the elliptic disk, circular disk, or ring resonator with an appropriate choice of the structural parameters.

The purpose of this paper, therefore, is to present a quasi-static analysis of an elliptic microstrip ring resonator. The capacitance of the structure is first determined with the spectral domain technique. It is utilized then to quantitatively assess the effect of fringing of the fields associated with the edges in terms of the effective parameters of the structure. The resonant frequency is determined, taking into account the effective values of the eccentricities of the inner and outer ellipses, the effective values of the ratio of the semimajor and semiminor axes, and the effective dielectric constant. The resonant frequency obtained with this theory is verified with the experiments. Mode charts for the dominant and higher order even and odd resonance modes are also presented.

II. Analysis

The elliptic microstrip ring resonator on a dielectric substrate of thickness d above the ground plane is shown in Fig. 1 along with the elliptic coordinate system ξ, η, and z. The outer ellipse with eccentricity e_0 and the inner ellipse with eccentricity e_1 form a confocal elliptic microstrip ring resonator. The focal distance between the focal points F and F' is $2h$, and is related to other structural parameters via the relation

$$2h = 2a_0e_0 = 2a_1e_1 \tag{1}$$

where a_0 and a_1 are the semimajor axes of the outer and inner ellipses, respectively. Alternatively, the eccentricities e_0 and e_1 also are expressed as

$$e_0 = \sqrt{1-(b_0/a_0)^2} \tag{2}$$

and

$$e_1 = \sqrt{1-(b_1/a_1)^2} \tag{3}$$

where b_0 and b_1 are the semiminor axes of the outer and inner ellipses, respectively. The axial coordinates of the outer and inner ellipses are ξ_0 and ξ_1.

The analysis of the elliptic microstrip ring resonator is performed with the quasi-static formulation of the spectral domain technique [12]. This technique has been extensively utilized in the evaluation of the discontinuity capacitance of various microstrip structures. From the quasi-static capacitance, the effective parameters of an equivalent structure with perfect magnetic walls can be calculated. The resonant frequency then is calculated for this structure. It has been observed for various structures [3]–[6] that this procedure is capable of providing fairly accurate resonant frequency within the range of quasi-static approximation.

Since the mathematical formulation of this structure is essentially similar to the one given earlier by Sharma and Bhat [6], we shall present only a terse mathematical description in the notation of [6].

The two-dimensional Fourier transform of the potential with respect to x- and y-axes is defined via the equation

$$\tilde{\phi}(\alpha,\beta,z) = \int_{-\infty}^{\infty}\int_{-\infty}^{\infty} \phi(x,y,z)\, e^{j(\alpha x+\beta y)}dxdy \tag{4}$$

where the potential function $\phi(x,y,z)$ satisfies Poisson's equation for a given charge density distribution $\rho(x,y)$ on the structure

$$\nabla^2\phi(x,y,z) = -\frac{1}{\epsilon}\rho(x,y)\delta(z-d). \tag{5}$$

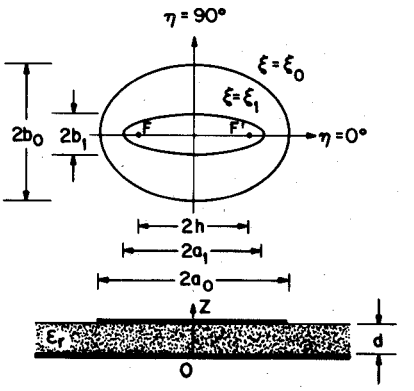

Fig. 1. A confocal elliptic microstrip ring resonator.

With the application of boundary conditions, the potential $\tilde{\phi}(\alpha,\beta,d)$ and the charge density $\tilde{\rho}(\alpha,\beta)$ at the interface are related by

$$\tilde{\phi}(\alpha,\beta,d) = \tilde{G}(\alpha,\beta,d)\tilde{\rho}(\alpha,\beta) \tag{6}$$

where $\tilde{G}(\alpha,\beta,d)$ is the Fourier transform of the Green's function. This is expressed as

$$\tilde{G}(\alpha,\beta,d) = \left[\epsilon_0\gamma(1+\epsilon_r\coth\gamma d)\right]^{-1} \tag{7}$$

with

$$\gamma = \left(\alpha^2+\beta^2\right)^{1/2}. \tag{8}$$

The charge density distribution is expressed in terms of basis functions $\rho_n(x,y)$ with unknown coefficients d_n. It is written in the Fourier transform domain as

$$\tilde{\rho}(\alpha,\beta) = \sum_{n=1}^{N} d_n\tilde{\rho}_n(\alpha,\beta). \tag{9}$$

The unknown coefficients d_n in (9) are determined from the solution of the matrix equation [3]

$$\sum_{n=1}^{N} d_n\langle\tilde{G}(\alpha,\beta,d)\tilde{\rho}_n(\alpha,\beta), \rho_m^*(\alpha,\beta)\rangle = (2\pi)^2\langle\phi_i(x,y,d), \rho_m(x,y)\rangle \tag{10}$$

which is derived with the application of Galerkin's method and Parseval's theorem. The capacitance of the structure is then obtained as

$$C = \sum_{n=1}^{N} d_n\int_E\int \rho_n(x,y)\, dxdy. \tag{11}$$

The charge density distribution function in (9) requires the Fourier transform of various basis functions $\rho_n(x,y)$. It can be easily deduced for microstrip structures of simple geometrical shapes. However, in general, for microstrip structures of complex shapes, it cannot be expressed easily in an analytical form. This invariably leads to considerable computation time required for the solution. Therefore, it is prudent to restrict the number of basis functions to a few to retain the numerical efficiency of this technique. In the present case, however, we shall assume only a uniform charge density distribution on the elliptic ring. At this point, it should be noted that the first-order variation in the representation of the charge density results in the second-order variation in the capacitance due to the variational nature of this technique [12]. Thus we write

$$\rho_1(x,y) = \begin{cases} 1, & \text{on } E \\ 0, & \text{elsewhere} \end{cases} \tag{12}$$

where the region E is the surface bounded by the following equations:

$$x^2/a_0^2 + y^2/b_0^2 = 1$$
$$x^2/a_1^2 + y^2/b_1^2 = 1. \tag{13}$$

The Fourier transform of (12), obtained using the procedure given in [13], is written as

$$\tilde{\rho}(\alpha,\beta) = \pi a_0 b_0 \left[1 - \frac{1}{4}\frac{p_0}{1!2!} + \frac{1}{4^2}\frac{p_0^2}{2!3!} - \frac{1}{4^3}\frac{P_0^3}{3!4!} + \cdots\right] - \pi a_1 b_1 \left[1 - \frac{1}{4}\frac{p_1}{1!2!} + \frac{1}{4^2}\frac{p_1^2}{2!3!} - \frac{1}{4^3}\frac{p_1^3}{3!4!} + \cdots\right] \tag{14}$$

with

$$p_0 = \left(\alpha^2 a_0^2 + \beta^2 b_0^2\right) \tag{15}$$

and

$$p_1 = \left(\alpha^2 a_1^2 + \beta^2 b_1^2\right). \tag{16}$$

The Fourier transform of the charge density given by (14) is utilized to evaluate the unknown coefficient d_1(with $N=1$) from the solution of the algebraic equation (10). The capacitance C of the structure is then calculated by (11). This is normalized with respect to the parallel-plate capacitance of the structure C_0 so that

$$C_N = C/C_0 \tag{17}$$

where

$$C_0 = \epsilon_0 \epsilon_r \pi (a_0 b_0 - a_1 b_1)/d. \tag{18}$$

The quasi-static resonant frequency is computed utilizing the concept of the effective dielectric constant (ϵ_{eff}) and the effective parameters of the structure. The effective dielectric constant is given by the ratio of the capacitance of the structure with the dielectric substrate to that with the dielectric substrate removed. That is

$$\epsilon_{\text{eff}} = \frac{C(\epsilon = \epsilon_0 \epsilon_r)}{C(\epsilon = \epsilon_0)}. \tag{19}$$

The effective parameters of the structure can be expressed in terms of the quasi-static capacitance. To that end, the area of the elliptic ring is written as

$$A = 2\pi h^2 (\sinh 2\xi_0 - \sinh 2\xi_1). \tag{20}$$

Consider now a hypothetical elliptic ring resonator having no fringe effects. Let the structural parameters in the notation of Fig. 1 be a_0', b_0', a_1', and b_1'. The capacitance of this structure is then given simply by

$$C_h = \epsilon_0 \epsilon_r \pi \left(a_0' b_0' - a_1' b_1'\right)/d. \tag{21}$$

The effective parameters can now be deduced when C_h equals C, which is the value of the capacitance derived using (11). Thus

$$C_N = \frac{C_h}{C_0} = \frac{\left(a_0' b_0' - a_1' b_1'\right)}{(a_0 b_0 - a_1 b_1)} \tag{22}$$

which can be written using (20) as

$$C_N = \frac{\cosh\left(\bar{\xi}_0 + \bar{\xi}_1\right)\sinh\left(\bar{\xi}_0 - \bar{\xi}_1\right)}{\cosh\left(\xi_0 + \xi_1\right)\sinh\left(\xi_0 - \xi_1\right)}. \tag{23}$$

We now define that

$$\xi_m = \frac{1}{2}(\xi_0 + \xi_1) = \frac{1}{2}\left(\bar{\xi}_0 + \bar{\xi}_1\right) \tag{24}$$

and

$$\bar{\xi}_d = \frac{1}{2}\left(\bar{\xi}_0 - \bar{\xi}_1\right) = \frac{1}{2}(\xi_0 - \xi_1) + \Delta\xi = \xi_d + \Delta\xi \tag{25}$$

which reduces (23) to

$$\Delta\xi = \frac{1}{2}\sinh^{-1}[C_N \sinh 2\xi_d] - \xi_d. \tag{26}$$

The corrected values of the axial coordinates are then

$$\bar{\xi}_0 = \xi_0 + \Delta\xi$$
$$\bar{\xi}_1 = \xi_1 - \Delta\xi. \tag{27}$$

The transverse magnetic (TM) fields existing on an elliptic microstrip ring resonator are dual of the transverse electric (TE) fields in an elliptic coaxial waveguide whose cross section is the same as that of the resonator shape. The eigenvalue equations for determining the cutoff wavenumbers of the TE and TM modes in an elliptic coaxial waveguide have been presented by Bräckelmann [14]. The relevant equations for the TM modes in an elliptic microstrip resonator are as follows.

Even modes, TM_{cmnp}:

$$Ce_m'(\xi_0, q_{cmn})\, Fey_m'(\xi_1, q_{cmn}) - Ce_m'(\xi_1, q_{cmn})\, Fey_m'(\xi_0, q_{cmn}) = 0 \tag{28}$$

Odd modes, TM_{smnp}:

$$Se_m'(\xi_0, q_{smn})\, Gey_m'(\xi_1, q_{scm}) - Se_m'(\xi_1, q_{smn})\, Gey_m'(\xi_0, q_{smn}) = 0 \tag{29}$$

where $Ce_m(\xi, q)$ and $Se_m(\xi, q)$ are the even and odd modified Mathieu functions of the first kind and order m. $Fey_m(\xi, q)$ and $Gey_m(\xi, q)$ are the even and odd modified Mathieu functions of the second kind and order m [15]. The primes in (28) and (29) denote the derivatives with respect to the argument ξ.

The wavenumber for the radial resonance is determined from the numerical solution of (28) and (29) for the nth parametric zero q_{cmnp} for the even mode and q_{smnp} for the odd mode. Thus

$$f_0 = \frac{c\sqrt{q}}{\pi\sqrt{\epsilon_{\text{eff}}}\, a_0' e_0'} \tag{30}$$

where f_0 is the resonant frequency, c is the velocity of light, and q is equal to q_{cmnp} and q_{smnp} for the even and odd modes, respectively.

III. Numerical Results

Following the foregoing analysis, a computer program was developed to solve the algebraic equation (10) in the spectral domain. The Fourier transform of the charge density, as given in (14), was evaluated with an accuracy of four significant digits or more. The integral on the left-hand side of (10) was evaluated as an iterated multiple integral using Gaussian quadrature. The convergence of the integral was also checked for various values of the structural parameters.

The capacitance of the structure then was evaluated with (11) for various values of the eccentricity of the outer ellipse and the ratio of the semiminor axes b_1/b_0. The normalized capacitance C_N as a function of d/a_0 obtained using (17) are depicted in Fig. 2. In Fig. 2(a), it is shown for a fixed value of $b_1/b_0 = 0.4$ and various values of $e_0 = 0.2$ (0.2) 0.8. In Fig. 2(b), it is shown for a fixed value of $e_0 = 0.4$ and $b_1/b_0 = 0.2$ (0.2) 0.8. The variation of C_N for various values of the dielectric constants $\epsilon_r = 1.0$, 2.22, 6.0, and 10.2 is plotted in Fig. 2(c) for $e_0 = 0.4$ and $b_1/b_0 = 0.4$. From these curves we observe that, for a fixed value of d/a_0, C_N

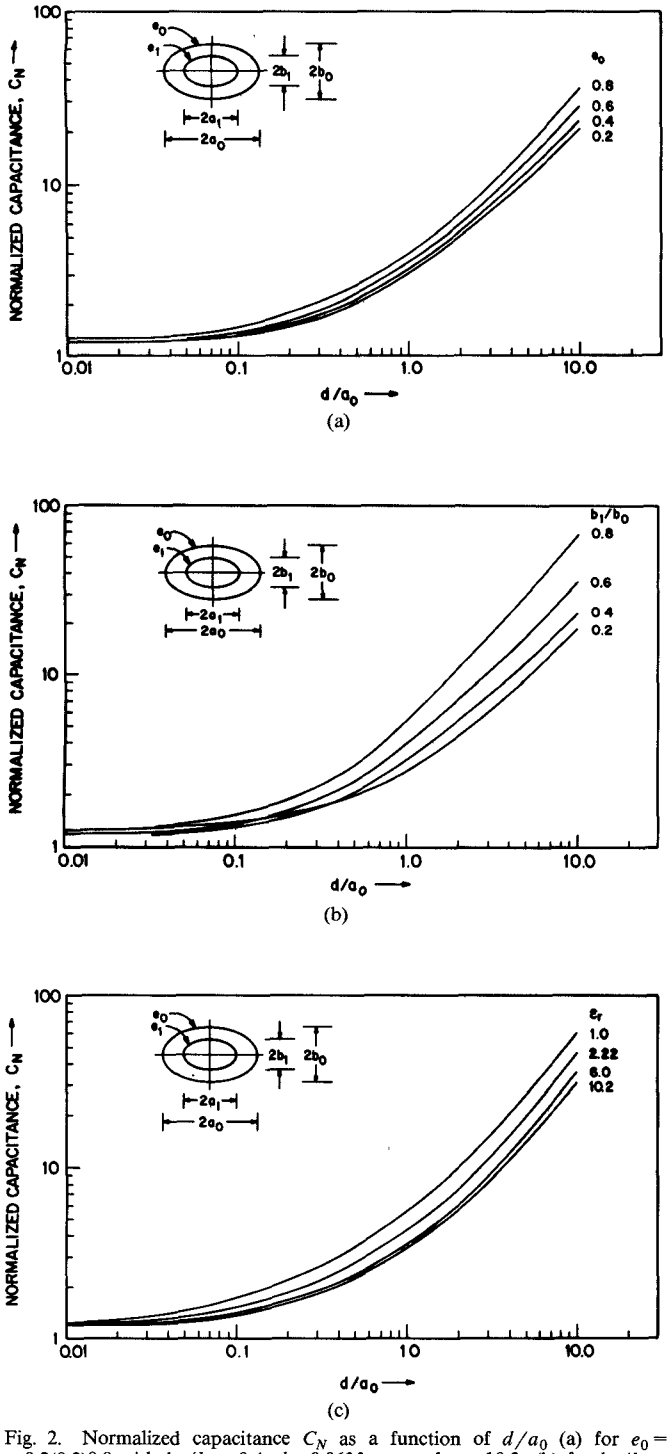

Fig. 2. Normalized capacitance C_N as a function of d/a_0 (a) for $e_0 = 0.2(0.2)0.8$ with $b_1/b_0 = 0.4$, $d = 0.0635$ cm, and $\epsilon_r = 10.2$; (b) for $b_1/b_0 = 0.2(0.2)0.8$ with $e_0 = 0.4$, $d = 0.0635$ cm, and $\epsilon_r = 10.2$; (c) for $\epsilon_r = 1.0$, 2.22, 6.0, 10.2 with $e_0 = 0.4$, $b_1/b_0 = 0.4$, and $d = 0.0635$ cm.

increases with an increase in e_0 or b_1/b_0 when the other parameters are kept fixed. C_N decreases as ϵ_r increases for fixed values of b_1/b_0 and e_0.

From the capacitance value, the end effects associated with an elliptic microstrip ring resonator are evaluated using the procedure presented in the previous section. This effect is determined in terms of 1) the effective values of the ratio of the semimajor and semiminor axes, 2) the effective values of the eccentricities of the inner and outer ellipses, and 3) the effective dielectric constant. All these effective parameters are useful in the evaluation of a theoretical value of the resonant frequency.

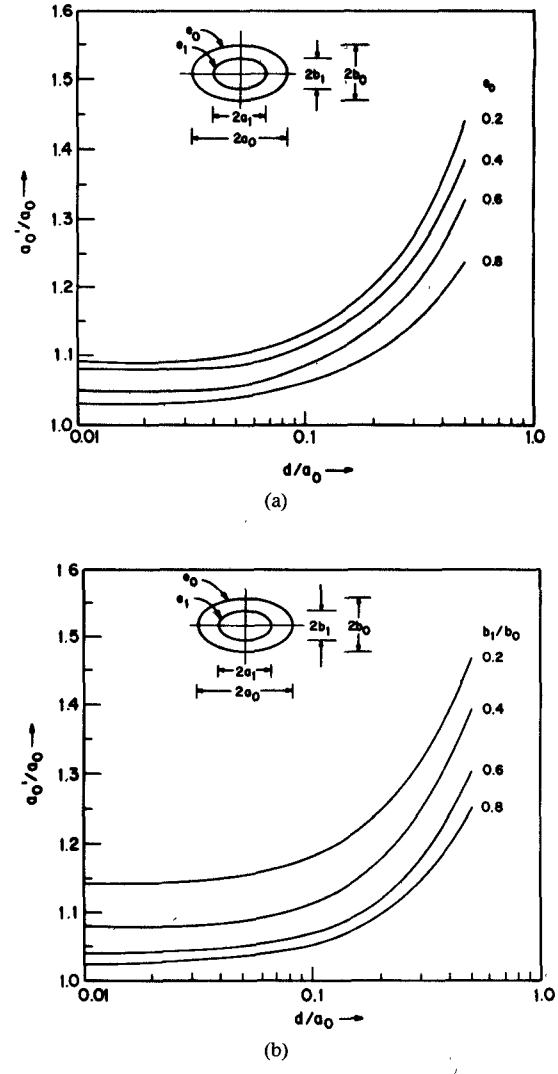

Fig. 3. Variation of the effective value of the ratio of the semimajor axes a_0'/a_0 as a function of d/a_0 (a) for $e_0 = 0.2$ (0.2)0.8 with $b_1/b_0 = 0.4$; (b) for $b_1/b_0 = 0.2(0.2)0.8$ with $e_0 = 0.4$. $d = 0.0635$ cm, and $\epsilon_r = 10.2$.

The variation of the effective value of the ratio of the semimajor axes a_0'/a_0 is shown in Fig. 3(a) and (b) as a function of d/a_0 for a fixed value of b_1/b_0 and e_0, respectively. As seen there, a_0'/a_0 decreases with an increase in either e_0 or b_1/b_0.

The variation of the effective dielectric constant (ϵ_{eff}) as a function of d/a_0 is shown in Fig. 4(a) for different values of e_0, and in Fig. 4(b) for different values of b_1/b_0. The effective dielectric constant is seen to decrease with an increase in d/a_0. It also decreases with an increase in either e_0 or b_1/b_0. For very small values of d/a_0, ϵ_{eff} is observed to be close to the static value ϵ_r.

The effective eccentricities of the inner and outer ellipses are plotted in Fig. 5(a) and (b), respectively, for $e_0 = 0.2$ (0.2) 0.8, and $d/a_0 = 0.05$ and 0.1. As b_1/b_0 is increased, e_0' increases while e_1' decreases. The effective value of b_1'/b_0', as shown in Fig. 5(c) for $b_1/b_0 = 0.2$ (0.2) 0.8, $d/a_0 = 0.05$ and 0.1, is seen to decrease with an increase in e_0.

The theoretical values of the resonant frequency in the even and odd radial resonance modes require resonance wavenumbers for the structure with effective parameters. This is evaluated by first solving the eigenvalue equations (28) and (29) for the parametric zero q_{cmnp} and q_{smnp} for given values of m, n, and p [16]. In Fig. 6(a)–(d), the mode characteristics of TM_{cmnp} and TM_{smnp} modes as a function of the eccentricity of the outer ellipse for

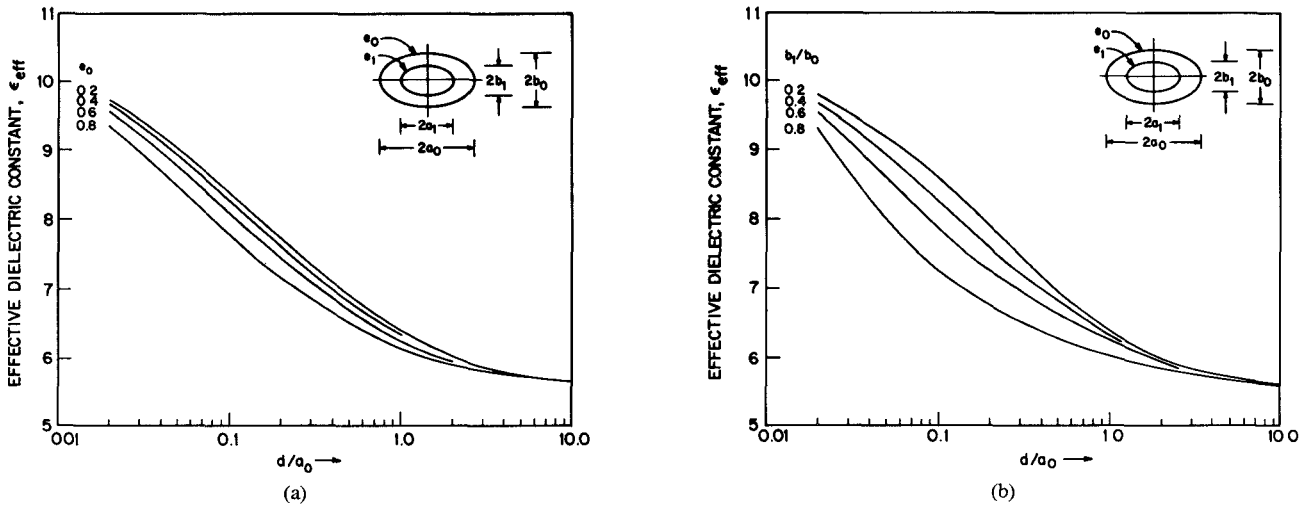

Fig. 4. Effective dielectric constant versus d/a_0 (a) for $e_0 = 0.2(0.2)0.8$ with $b_1/b_0 = 0.4$; (b) for $b_1/b_0 = 0.2(0.2)0.8$ with $e_0 = 0.4$. $d = 0.0635$ cm, and $\epsilon_r = 10.2$.

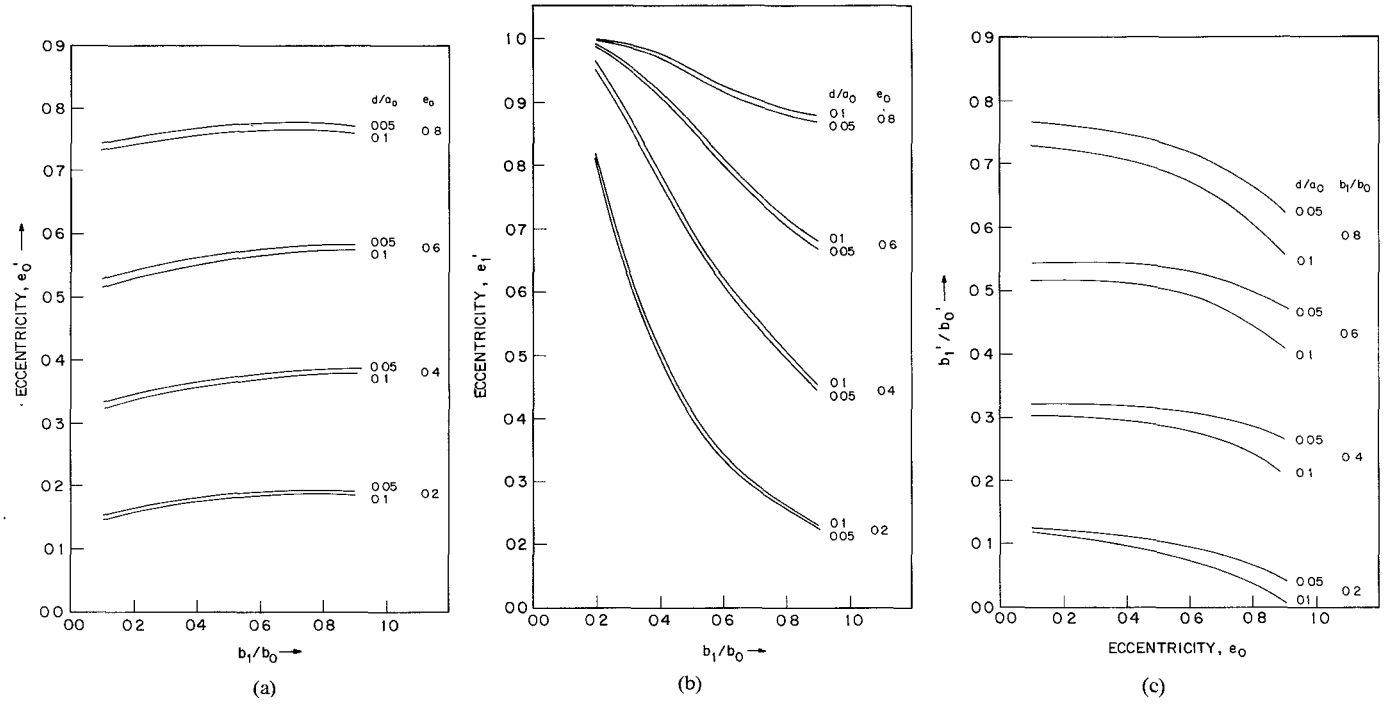

Fig. 5. The effective value of the eccentricity of (a) the outer ellipse e_0', (b) the inner ellipse e_1' as a function of b_1/b_0 for values of $d/a_0 = 0.05$, 0.1, and $e_0 = 0.2(0.2)0.8$, and (c) the effective ratio of the semiminor axes b_1'/b_0' as a function of the eccentricity of the outer ellipse e_0 for values of $d/a_0 = 0.05$, 0.1, and $b_1/b_0 = 0.2(0.2)0.8$. $d = 0.0635$ cm, $\epsilon_r = 10.2$.

various values of the ratio of the semiminor axes are displayed for $m = 1$ to 4 with $n = 1$ and $p = 0$. From these graphs we observe that, when e_0 is equal to zero, the value of ka_0 is the same in the even and odd resonance modes. For a confocal elliptic microstrip ring resonator, e_0 equals zero implies that e_1 is also zero. It becomes a circular ring resonator with b_1/b_0 as the ratio of the inner to outer radius. As e_0 is further increased, ka_0 increases for the even TM_{cmnp} modes. Depending on the value of b_1/b_0, it either decreases or increases in the odd TM_{smnp} modes. In all cases, however, increasing the ratio of the semiminor axes b_1/b_0 for a fixed value of e_0 causes a decrease in the value of ka_0. Furthermore, ka_0 in the even TM_{cmnp} mode is always greater than the corresponding value in the odd TM_{smnp} mode for $e_0 > 0$. This leads us to conclude that the odd TM_{s110} mode is the dominant mode for the elliptic microstrip resonator. It is consistent also with the results presented by Bräckelmann [14] for the even and odd TE mode cutoff wavenumbers of a coaxial waveguide of elliptic cross section.

The current distribution on the elliptic microstrip ring resonator is deductively derived from the electromagnetic fields existing in the coaxial elliptic waveguide [14]. It is depicted in Fig. 7(a) and (b) for the even TM_{c110} and odd TM_{s110} modes, respectively. As shown there, the even mode is obtained when the resonator is excited along the major axis ($\eta = 0°$), while the odd mode is obtained when it is excited along the minor axis ($\eta = 90°$).

Using the effective values of the structural parameters, the theoretical resonant frequency was evaluated and compared with the experiment. The elliptic microstrip ring resonators were

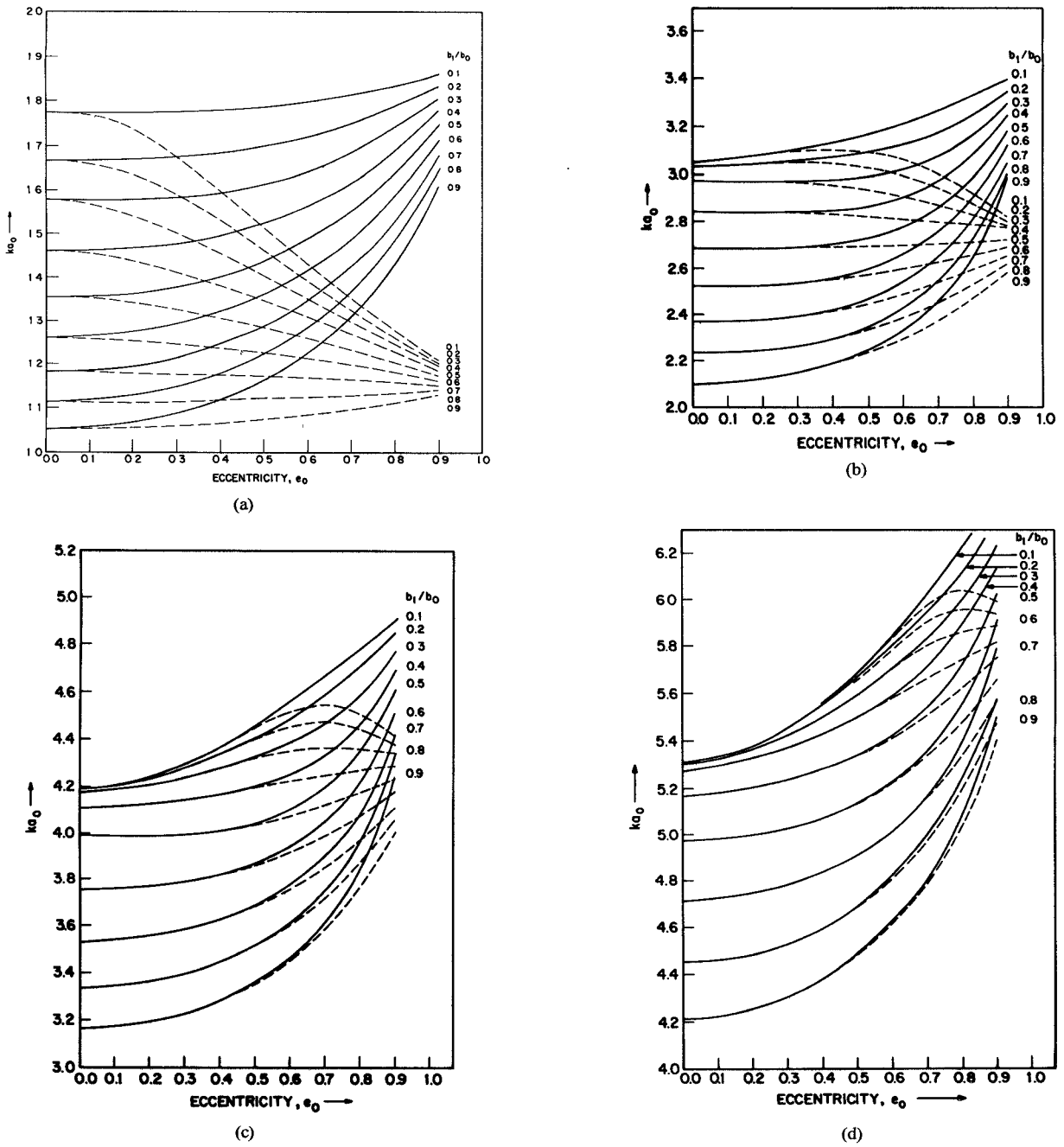

Fig. 6. Mode charts for the confocal elliptic microstrip resonator in the even TM_{cmnp} and odd TM_{smnp} modes; ka_0 as a function of e_0. b_1/b_0 is a variable. ——— TM_{cmnp} ------ TM_{smnp} for $n=1$, $p=0$ and (a) $m=1$; (b) $m=2$; (c) $m=3$; (d) $m=4$.

fabricated on Epsilam-10 ($\epsilon_r = 10.2$) substrates. The resonators were coupled through a 50-Ω microstripline along the semimajor axis. The coupling to the resonator was adjusted to an optimum value such that the influence of the coupling gap on the resonant frequency was negligible. This value of the coupling gap then was used throughout the experiments. Due to this excitation, only the even TM_{c110} mode was excited. The theoretical and experimental verification of the resonant frequency of this mode was performed for two cases. In the first case, the semimajor axis a_0 was increased from 0.2 to 0.7 cm for a fixed value of $e_0 = 0.5$ and $b_1/b_0 = 0.5$. In the second case, for each value of the eccentricity of the outer ellipse $e_0 = 0.2$ to 0.8, the ratio of semiminor axes b_1/b_0 was varied between 0.2 to 0.8 in steps of 0.2. The theoretical resonant frequency for the even TM_{c110} mode was calculated from the parametric zero obtained using the effective parameters e_0' and b_1'/b_0'. The results for the first case are shown in Fig. 8(a), and that of the second case are shown in Fig. 8(b). The experimental values are also displayed there. The agreement between theoretical and experimental resonant frequency was observed to be within typically ±2 percent in the frequency range of 2 to 12 GHz.

IV. Conclusions

In this paper, we have presented a complete analysis of the elliptic microstrip ring resonator. This is a general resonant structure which reduces to an elliptic disk when $b_1/b_0 = 0$, a circular ring when $e_0 = 0$, and a circular disk when both $e_0 = 0$ and $b_1/b_0 = 0$. The quasi-static capacitance of this structure was obtained for various dielectric constants and structural parameters. The effective dielectric constant was determined from the

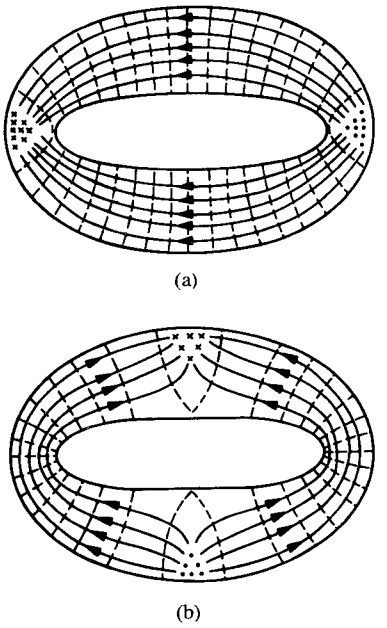

Fig. 7. Field patterns on an elliptic microstrip ring resonator in (a) TM_{c110} mode, (b) TM_{s110} mode. oooo xxxx Electric field, ------- Magnetic Field, ——— Currents on the top plate.

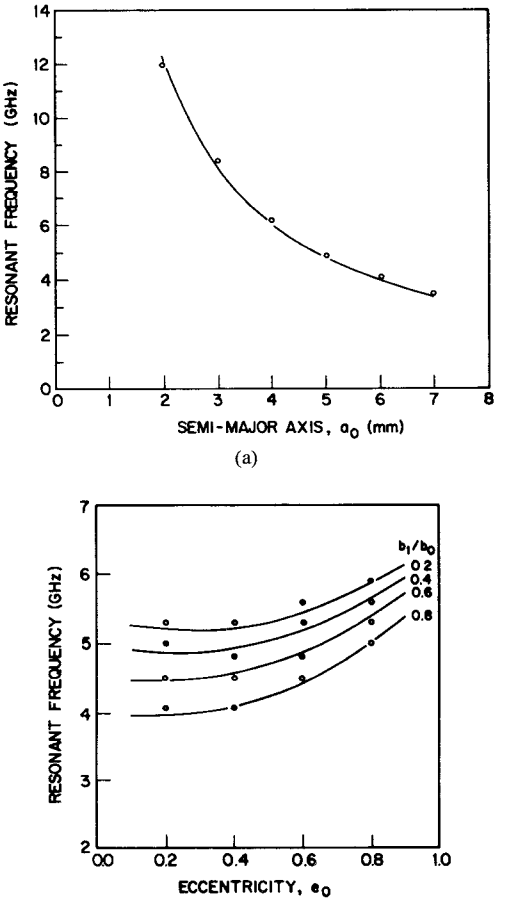

Fig 8. Theoretical and experimental resonant frequency as a function of (a) semimajor axis a_0 for $e_0 = 0.5$ and $b_1/b_0 = 0.5$; (b) eccentricity with $2a_0 = 1.0$ cm. $d = 0.0635$ cm, $\epsilon_r = 10.2$. ——— this theory, o o o o o experiment

ratio of the capacitance with and without the dielectric substrate. A procedure for evaluating the end effects associated with the fringing of fields in terms of the effective values of the eccentricities of the outer and inner ellipses, and the effective values of the semimajor and semiminor axes, was presented. The resonant frequency utilizing the effective structural parameters was found also to agree within typically ± 2 percent up to about 12 GHz. This is reasonable in view of the fabrication tolerances and the variations in the value of the dielectric constant. Mode charts for the confocal elliptic microstrip ring resonators were also presented for the first four even and odd radial resonance modes. It is believed that these results would provide much-needed information in the design of elliptic microstrip ring resonators.

Acknowledgment

The author would like to thank Dr. S. R. Rengarajan of California State University, Northridge, CA, for his helpful suggestions.

References

[1] J. Helszajn and D. S. James, "Planar triangular resonators with magnetic walls," *IEEE Trans. Microwave Theory Tech.*, vol. MTT-26, pp. 95–100, Feb. 1978.

[2] A. K. Sharma and B. Bhat, "Analysis of triangular microstrip resonators," *IEEE Trans. Microwave Theory Tech.*, vol. MTT-30, pp. 2029–2031, Sept. 1982.

[3] A. K. Sharma and W. J. R. Hoefer, "Spectral domain analysis of an hexagonal microstrip resonator," *IEEE Trans. Microwave Theory Tech.*, vol. MTT-30, pp. 825–828, May 1982.

[4] A. K. Sharma and B. Bhat, "Spectral domain analysis of microstrip ring resonators," *Arch. Elek. Übertragung.*, vol. 33, pp. 130–132, Mar. 1979.

[5] A. K. Sharma and B. Bhat, "Influence of shielding on the capacitance of shielded microstrip disk and ring structures," *Arch. Elek. Übertragung.*, vol. 34, pp. 41–44, Jan. 1980.

[6] A. K. Sharma and B Bhat, "Spectral domain analysis of elliptic microstrip disk resonators," *IEEE Trans. Microwave Theory Tech.*, vol. MTT-28, pp. 573–576, June 1980.

[7] R. T. Irish, "Elliptic resonator and its use in microcircuit systems," *Electron. Lett.*, vol. 7, pp. 149–150, Apr 1971.

[8] J. G. Kretzschmar, "Theoretical results for the elliptic microstrip resonator," *IEEE Trans. Microwave Theory Tech.*, vol. MTT-20, pp. 342–343, May 1972.

[9] L. C. Shen, "The elliptic microstrip antenna with circular polarization," *IEEE Trans. Antennas and Prop*, vol. AP-29, pp. 90–94, Jan. 1981

[10] J. G. Kretzschmar, "Theory of the elliptic disk and ring resonator," in *Proc. Fifth Colloquium on Microwave Communication*, (Budapest, Hungry), June 24–30, 1974.

[11] J. G. Kretzschmar, "The elliptic microstrip ring resonator," in *Proc. Seventh European Microwave Conf.*, (Copenhagen, Denmark), Sept. 5–8, 1977, pp. 465–469.

[12] Y. Rahmat-Samii, T. Itoh, and R. Mittra, "A spectral domain analysis for solving microstrip discontinuity problems," *IEEE Trans. Microwave Theory Tech.*, vol. MTT-22, pp. 372–378, Apr. 1974.

[13] P. K. Mondal, "Franhaufer diffraction due to an elliptic annulus," *J Opt. Soc. Amer.*, vol. 65, pp. 1154–1156, Oct. 1975.

[14] W. Bräckelmann, "Die Grenzfrequenzen von hoheren Wellentypen im Koaxialkabel mit elliptischem Querschnitt," *Arch. Elek. Übertragung.*, vol. 21, pp. 421–426, Aug. 1967.

[15] N. W. McLachlan, *Theory and Application of Mathieu Functions* Oxford, England: University Press, 1951.

[16] S. R. Rengarajan and J. E. Lewis, "Mathieu functions of integral orders and real arguments," *IEEE Trans. Microwave Theory Tech.*, vol. MTT-28, pp. 276–277, Mar. 1980.